Gourvenec, S. (2007). *Géotechnique* **57**, No. 8, 637–646 **doi:** 10.1680/geot.2007.57.8.637

Shape effects on the capacity of rectangular footings under general loading

S. GOURVENEC*

Ultimate limit states under vertical (*V*), moment (*M*) and horizontal (*H*) loading of rectangular footings with varying breadth-to-length aspect ratios (*B*/*L*) are compared with predictions for plane-strain conditions. Footing/soil interfaces unable to sustain tension and with unlimited tensile resistance are considered. Finite element and analytical predictions are reported, and results are presented as failure envelopes in *VH*, *VM* and *VMH* load space. Vertical and moment capacity of rectangular footings, with either zero or unlimited tension interfaces, is shown to increase with reducing footing length, for foundations of a given bearing area. For footings unable to sustain tension, footing aspect ratio does not affect the shape of the failure envelope: therefore ultimate limit states of a footing of any aspect ratio can be derived from a unique envelope scaled by the appropriate ultimate limit loads defining its apex points. A closed-form expression is proposed to describe the shape of the normalised *VMH* envelope. The shape of failure envelopes for footings able to sustain tension is dependent on footing geometry.

KEYWORDS: bearing capacity; footings/foundations; numerical modelling

On compare les états limites ultimes aux charges verticale (*V*), au moment (*M*) et horizontale (*H*) de semelles rectangulaires présentant différents ratios sur le plan largeur /longueur (*B*/*L*) en formulant des prédictions pour les contraintes planes. On examine des interfaces semelle /sol incapables de soutenir la tension et présentant une résistance illimitée à la traction. On fournit des prédictions aux éléments finis et analytiques, et on présente des résultats sous forme d'enveloppes de rupture dans l'espace de charge *VH*, *VM* et *VMH*. On démontre que la capacité verticale et au moment de semelles rectangulaires, avec interfaces de tension nulle ou illimitée, augmente en fonction de la réduction de la longueur de la semelle, pour des fondations d'une certaine surface portante. Pour les semelles qui ne sont pas en mesure de soutenir la tension, le ratio d'aspect de la semelle n'affecte pas la forme de l'enveloppe de rupture : en conséquence, il est possible de dériver les états-limites ultimes d'un ratio d'aspect quelconque avec une enveloppe unique à échelle déterminée par les charges limites ultimes appropriées définissant ses sommets. On propose une expression à forme fermée pour décrire la forme de l'enveloppe *VMH* normalisée. La forme d'enveloppes de rupture, pour les semelles en mesure de soutenir la tension est fonction de la géométrie de la semelle.

INTRODUCTION

Ultimate limit states for footings under general loading are conventionally achieved by applying multiplicative modification factors to the classical plane-strain solution for vertical bearing capacity (Terzaghi, 1943). For undrained conditions the ultimate vertical bearing capacity q_{ult} of a surface footing can be expressed by

$$q_{ult} = \frac{V_{ult}}{A'} = N_c s_u s_c i_c \quad (1)$$

where N_c is the plane-strain bearing capacity factor ($2 + \pi$), s_u is the undrained shear strength of the soil, and s_c and i_c are modification factors to account for footing shape and load inclination respectively. A' is the effective area of the footing, and accounts for the reduction in bearing capacity due to moment.

Vertical load and moment is considered as a vertical load applied at an eccentricity $e = M/V$ from the footing centreline according to the effective width method (Meyerhof, 1953). The method relies on the assumption that a strip footing of breadth B, subjected to a vertical load V at an eccentricity e from its centreline has the same bearing capacity as a footing of effective width $B' = B - 2e$ subjected to the same vertical load centrally applied. It follows that a rectangular footing loaded in an orthogonal plane midway along its longitudinal axis has an effective area $A' = B'L$. (If V is applied with an eccentricity relative to the centreline of the longitudinal axis a similar correction is applied to the length dimension. In this study loading in the vertical plane midway along the longitudinal axis is considered, and so the additional correction is not relevant.)

For a rectangular footing of effective breadth B' and length L, a widely adopted shape factor is that proposed by Skempton (1951),

$$s_c = 1 + 0{\cdot}2\frac{B'}{L} \quad (2)$$

For a footing subjected to a horizontal load in conjunction with a vertical load, the vertical bearing capacity is adjusted by an inclination factor,

$$i_c = 0{\cdot}5 + 0{\cdot}5\sqrt{1 - \frac{H}{A's_u}} \quad (3)$$

where H is the component of horizontal load and A' is the effective area of the footing (i.e. $B'L$). Equation (3) is based on an algebraic fit to an exact solution for inclined loading (Green, 1954) given by

$$\frac{V}{As_u} = \left(1 + \frac{\pi}{2}\right) + \cos^{-1}\left(\frac{H}{As_u}\right) + \sqrt{1 - \left(\frac{H}{As_u}\right)^2} \quad (4)$$

where

$$\frac{H}{As_u} = 1 \text{ for } \frac{V}{As_u} \leqslant 0{\cdot}5$$

Conventional bearing capacity theory, as outlined above,

Manuscript received 2 February 2006; revised manuscript accepted 10 April 2007.
Discussion on this paper closes on 1 April 2008, for further details see p. ii.
* Centre for Offshore Foundation Systems, University of Western Australia.

implicitly treats a combination of vertical, moment and horizontal loading as an eccentrically applied inclined point load, with linear superposition of the solutions accounting for eccentricity and inclination. Ultimate limit states under general loading predicted by this method have previously been questioned in the light of analytical and numerical studies (Ukritchon *et al.*, 1998; Gourvenec, 2004). It is increasingly popular to predict undrained ultimate limit states under general loading explicitly, i.e. $f(V, M, H)$, and represent the collapse loads as a failure envelope in *VMH* load space (e.g. Bransby & Randolph, 1998; Ukritchon *et al.*, 1998; Martin & Houlsby, 2001; Taiebat & Carter, 2000, 2002; Gourvenec & Randolph, 2003; Gourvenec, 2004). The yield envelope approach in itself is not new (Roscoe & Schofield, 1957), and has been widely applied to drained bearing capacity problems (e.g. Butterfield & Ticof, 1979; Nova & Montrasio, 1991; Butterfield & Gottardi, 1994). Since yield and failure are synonymous for conditions of perfect plasticity, as considered in this study, the term 'failure envelope' (rather than yield envelope) is adopted.

Previous studies of undrained bearing capacity under general loading have addressed plane-strain conditions and circular footings, with an interface either unable to sustain tension or permitted to develop unlimited tension (e.g. Ukritchon *et al.*, 1998, consider a plane-strain footing with a zero-tension interface; Taiebat & Carter, 2002, consider a circular footing with a zero-tension interface; and Gourvenec & Randolph, 2003a, consider plane-strain and circular footings with fully bonded interfaces). These previous studies have shown that the mechanisms governing failure, and consequently the shape of the failure envelopes, differ for plane-strain and axisymmetric geometry for both zero-tension and unlimited tension interface conditions. As a result, ultimate limit states of a circular footing under general loading predicted by scaling an envelope derived for plane-strain conditions by the appropriate uniaxial ultimate limit states would be unreliable. Undrained failure of rectangular footings under general loading, with either zero or unlimited tension capacity, has not previously been considered. Mechanisms of failure under general loading of rectangular footings would be expected to be similar for varying aspect ratios, and similar to failure in plane strain (more so than a circular footing). If this is the case, ultimate limit states of rectangular footings of all aspect ratios could be predicted from a unique envelope scaled by the appropriate ultimate limit loads under pure vertical, moment and horizontal load.

Exact solutions for the uniaxial vertical bearing capacity of square or rectangular footings have yet to be found. As indicated in equation (2), a semi-empirical shape factor is conventionally applied to the vertical bearing capacity solution for plane-strain conditions to account for aspect ratio. The most commonly adopted expression, proposed by Skempton (1951), suggests a linear relationship between the ultimate vertical load and aspect ratio, with a maximum increase of 20% for a square footing compared with the plane-strain case (i.e. $s_c = 1{\cdot}2$).

Exact solutions for smooth and rough circular footings give $5{\cdot}69 < N_c < 6{\cdot}05$ (Cox *et al.*, 1961), corresponding to shape factors $1{\cdot}11 < s_c < 1{\cdot}18$. A shape factor of 1·2 for a square footing, as implied by equation (2) (Skempton, 1951), is counter-intuitive, contrary to expectation that the bearing capacity factors for square and rectangular footings would be bracketed by those for strip and circular geometries (Levin, 1955).

Analytical solutions for vertical bearing capacity of rough rectangular footings of various aspect ratios are reported by Michalowski (2001), Salgado *et al.* (2004) and Gourvenec *et al.* (2006), and are presented in Fig. 1, along with predictions from the empirical expression proposed by Skempton (1951). Considerable disparity between the different solutions is evident, and all the upper bounds predict bearing capacity factors for square footings above the exact solution for a circular footing.

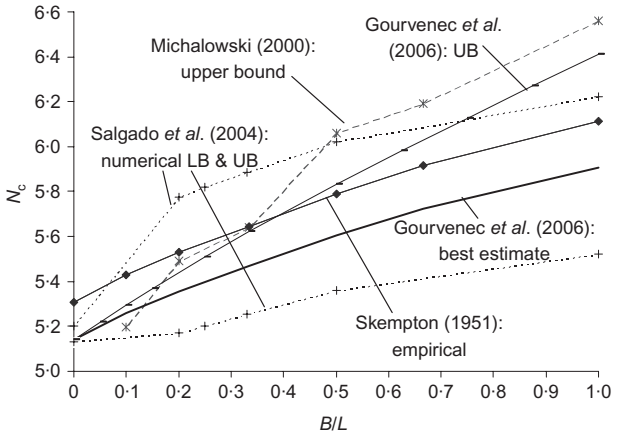

Fig. 1. Vertical bearing capacity factors for rectangular footings

A detailed review of the available literature of analytical and numerical studies addressing bearing capacity factors for square and rectangular footings is reported by Gourvenec *et al.* (2006). Based on results from finite element analyses, Gourvenec *et al.* (2006) propose best-estimate bearing capacity factors for rough rectangular footings, also shown in Fig. 1, which can be described by a quadratic function

$$N_c = (2 + \pi) + 1{\cdot}08\frac{B}{L} - 0{\cdot}2\left(\frac{B}{L}\right)^2 \tag{5}$$

or expressed in terms of a shape factor

$$s_c = 1 + 0{\cdot}214\frac{B}{L} - 0{\cdot}067\left(\frac{B}{L}\right)^2 \tag{6}$$

Equations (5) and (6) suggest a vertical bearing capacity $N_c = 5{\cdot}91$ for a square footing, in line with Levin's suggestion that the bearing capacity factors for square and rectangular footings would be bracketed by those for strip and circular geometries (Levin, 1955).

Moment capacity (M_{ult}) of footings unable to sustain tension is almost universally considered with the effective width method (Meyerhof, 1953). Moment capacity is predicted as a function of vertical load, as a result of which three-dimensional geometry can be simply incorporated through a shape factor applied to the vertical bearing capacity. Upper-bound solutions for strip and circular footings able to sustain unlimited tension have been derived based on rotational scoop mechanisms, contained beneath the footing and with a centre of rotation located some distance above the centre of the footing/soil interface. Murff & Hamilton (1993) set out the plastic work calculation for a rotational scoop, defined by a segment of a cylinder for plane-strain conditions and integrated over a spherical segment for a circular footing. These mechanisms of a plane circular scoop or spherical segment give optimum upper bounds for M_{ult}/ABs_u or $M_{ult}/ADs_u = 0{\cdot}69$ and 0·67 for plane-strain and circular footings respectively (Randolph & Puzrin, 2003). Logic suggests a cylindrical scoop would govern rotational failure of a rectangular footing, although this has not previously been verified by plasticity or numerical analysis.

Prediction of the ultimate undrained horizontal resistance (H_{ult}) of a surface footing is trivial: governed by sliding, it

depends only on the base area of the footing (A) and shear strength of the soil (s_u).

In this study ultimate limit states under general loading of rectangular footings with varying aspect ratio, and for conditions of plane strain, are investigated with finite element analyses. Footing/soil interfaces unable to sustain tension and permitted to mobilise unlimited tension are considered. Results are reported as failure envelopes in VMH load space in terms of dimensionless and normalised loads defining both their size and shape as a function of footing aspect ratio.

FINITE ELEMENT MODEL

All the finite element analyses were carried out using the software ABAQUS (HKS, 2002).

Mesh

The three-dimensional finite element mesh used for analysis of a square footing of width B and equal length L is shown in Fig. 2(a). It represents a half-footing cut through one of the orthogonal planes of symmetry. The mesh extends $3B$ from the edges of the footing and $2{\cdot}5B$ beneath the footing. Zero-displacement boundary conditions prevent out-of-plane displacements of the vertical boundaries, and the base of the mesh is fixed in all three coordinate directions.

Various different mesh densities were investigated to achieve a time-efficient model without compromising accuracy. The mesh shown in Fig. 2(a) comprises approximately 12 000 first-order fully integrated hexahedral hybrid elements. The hybrid element formulation uses a mixture of displacement and stress variables (as opposed to solely displacement) to approximate the equilibrium equations and compatibility conditions. Hybrid elements are recommended for modelling the response of near-incompressible materials (such as is appropriate for undrained soil conditions).

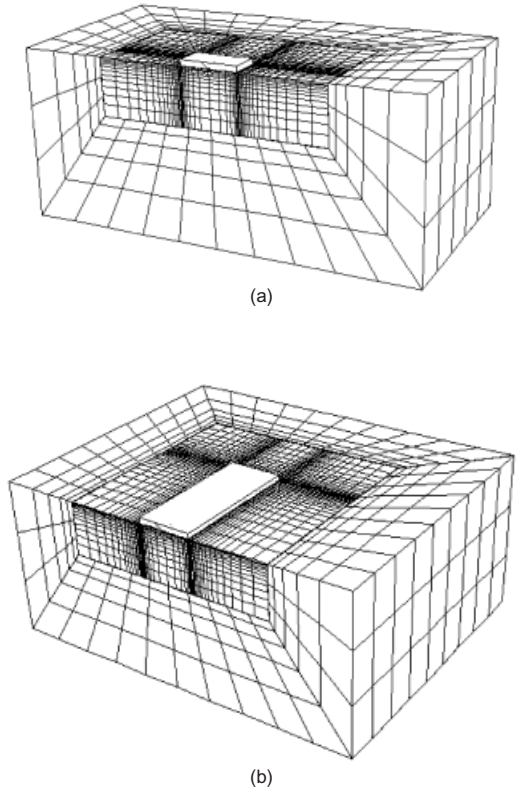

Fig. 2. Finite element meshes: (a) square footing, $L = B$; (b) rectangular footing with $L = 5B$

Six three-dimensional models were created to investigate the effect of varying footing breadth-to-length aspect ratio on bearing capacity ($B/L = 0{\cdot}1$, $0{\cdot}2$, $0{\cdot}33$, $0{\cdot}5$, $0{\cdot}67$ and 1 (square)). Each mesh represents a half-footing, measured along the longitudinal axis, and maintains the same geometry and discretisation on the front face of the mesh as for the square footing shown in Fig. 2(a). For the longer footings more elements were used in the longitudinal direction to maintain uniform element size across the models, and the rear mesh boundary was positioned sufficiently remotely not to affect footing behaviour. For example, the mesh for the $L = 5B$ footing (shown in Fig. 2(b)) comprises 18 000 elements, and the mesh for the $L = 10B$ footing comprises 25 000 elements (more than twice as many as the square footing mesh shown in Fig. 2(a)). A plane-strain mesh was also constructed using first-order fully integrated quadrilateral hybrid elements. The same geometry and discretisation as for the front face of the three-dimensional mesh were used, and equivalent boundary conditions, soil conditions and analysis procedures were modelled.

A vertical bearing capacity factor of $N_c = 5{\cdot}31$ was obtained from the plane-strain finite element analysis, over-predicting the exact solution by just 3%. A much finer plane-strain mesh was also constructed using 1500 elements, two and a half times as many elements as the coarser mesh. The finer mesh gave a vertical bearing capacity factor $N_c = 5{\cdot}27$, only a $0{\cdot}5$% increase in accuracy, indicating that the coarser mesh was sufficiently fine.

Material properties

Simple soil conditions were modelled representing an isotropic linear elastic-perfectly plastic material failing according to a Tresca yield condition with uniform undrained shear strength with depth s_u. The conditions considered are intended to represent a fine-grained material subjected to a period of loading sufficiently short that no drainage will take place. Constant stiffness index $E_u/s_u = 1000$, Poisson's ratio $\nu = 0{\cdot}49$, and buoyant unit weight $\gamma' = 8\ \mathrm{kN/m^3}$ were prescribed. Although soil self-weight was used in the analysis, the nature of the problem considered (a surface footing resting on an isotropic homogeneous soil without drainage) leads to the calculated bearing capacity being unaffected by the value of γ'.

The footing was represented as a discrete rigid body resting on the surface of the soil. The interface between the footing and the soil was either fully bonded (no slip or separation between the footing and soil permitted) or represented by a contact surface. The contact surface modelled a rough interface, prescribed a shear resistance equal to the undrained shear strength of the soil. Normal to the interface, separation was permitted when the contact pressure fell below zero.

Load paths

Constant-ratio displacement probe tests and displacement-controlled swipe tests were carried out. The footing was subjected to controlled displacements, as opposed to directly applied loads, to enable post-failure conditions to be observed. The reference point for the applied displacement was taken as the midpoint of the footing base.

Each analysis followed a single displacement-controlled load path to failure. For pure vertical (V), horizontal (H) and moment (M) loading displacements w, u and θ respectively were imposed; for the combined load cases VH, VM and HM (in planes $M = 0$, $H = 0$ and $V = 0$ respectively),

displacements were imposed at a fixed displacement ratio w/u, w/θ and u/θ. For combinations of vertical, moment and horizontal load (*VMH*), a constant vertical load was imposed as a direct force, and the horizontal and moment load components were imposed at a fixed displacement ratio (u/θ). Combinations of negative and positive horizontal load in conjunction with positive moment were investigated, as the response to combined horizontal load and moment acting in the same direction (i.e. clockwise and left to right, or vice versa) differs from that when the horizontal load and moment act in opposition (i.e. clockwise and right to left, or vice versa). This is in contrast to *VH* and *VM* loading, where symmetry of the problem indicates that $f(V, H) = f(V, -H)$ or $f(V, M) = f(V, -M)$, so that only load combinations with $V \geqslant 0$ and H or $M \geqslant 0$ are required to define the complete failure envelope.

The probe tests give rise to load paths that move from the origin across the failure envelope, initially at gradients determined by the elastic stiffness but with the gradients changing owing to internal plastic yielding as the paths approach the failure envelope. Once the failure envelope is reached, each loading path travels around the failure envelope until it reaches a point where the normal to the failure envelope matches the prescribed displacement ratio. A bounding failure envelope is defined by interpolation between terminating points of a selection of probe tests.

Swipe tests (introduced by Tan, 1990) were also carried out to identify the failure envelopes in *VH* and *VM* space. The footing was first brought to failure with uniaxial vertical displacement followed by a translational or rotational swipe (u, θ) at constant vertical displacement. The benefit of the swipe test is that a complete failure locus on a certain plane can be determined in a single test. Previous studies of strip and circular footings have confirmed that swipe paths track very close to the failure envelopes in planes of $M = 0$ and $H = 0$ with good agreement between constant-ratio displacement probe tests, but are unsuitable for loading in the $V = 0$ plane (Bransby & Randolph; 1998, Gourvenec & Randolph, 2003a).

Sign convention and nomenclature

The sign convention for displacements and loads presented in this paper obeys a right-handed axes and clockwise positive convention as proposed by Butterfield *et al.* (1997), as shown in Fig. 3. The load reference point and notation for footing geometry and spacing are also defined in Fig. 3.

The notation adopted for loads and displacements is defined in Table 1. The ultimate loads are those for pure loading (e.g. $H = M = 0$ for V_{ult}). This is important in respect of moment loading for footings able to sustain tension, where the maximum moment is mobilised under conditions where $H > 0$. The maximum moment will be denoted by M_{max} (and corresponding $m_{max} = M_{max}/M_{ult}$).

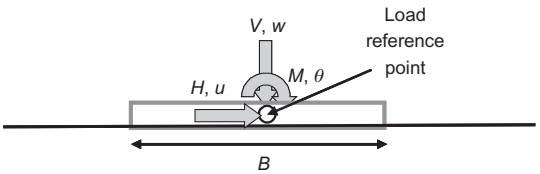

Fig. 3. Sign convention and nomenclature; positive loads shown

RESULTS

Failure envelopes are presented in *VH*, *VM* and *VMH* load space. For each footing aspect ratio modelled, the swipe tests and constant-ratio displacement probe tests defined the same failure envelope in planes of $M = 0$ and $H = 0$, and the swipe paths are presented. The failure envelopes in the *HM* plane are derived from $u{:}\theta$ constant-ratio displacement probe tests at selected vertical loads as swipe tests were known to be unsuitable even in the $V = 0$ plane (Gourvenec & Randolph, 2003a).

VH loading plane ($M = 0$)

Failure envelopes in vertical and horizontal load space ($M = 0$) are shown in Fig. 4 for each of the footing geometries modelled: $B/L = 0$ (plane strain), 0·1, 0·2, 0·33, 0·5, 0·67 and 1 (square).

The expansion of the failure envelopes in Fig. 4(a) indicates the increased load capacity with increasing footing aspect ratio. The failure envelopes expand along the vertical load axis, in line with equation (5), while the ultimate unit

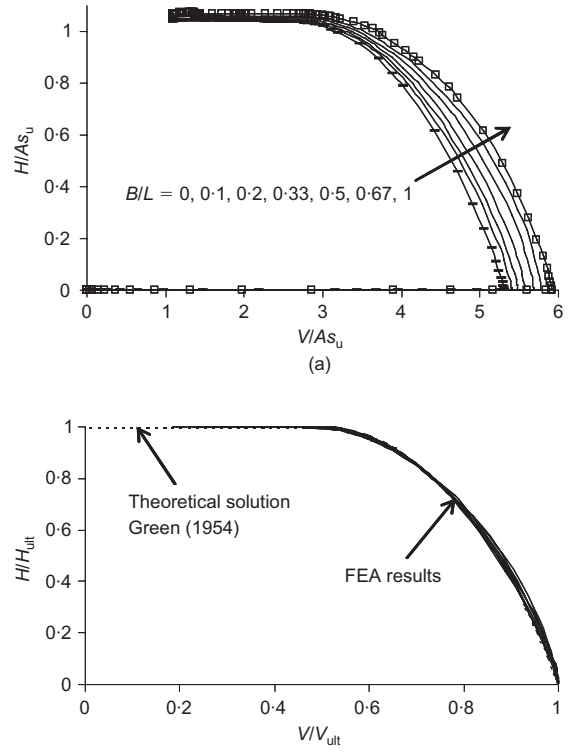

Fig. 4. Failure envelopes for *VH* loading ($M = 0$): (a) dimensionless load space; (b) normalised load space

Table 1. Summary of notation for loads and displacements

	Vertical	Horizontal	Rotational
Load	V	H	M
Ultimate load	V_{ult}	H_{ult}	M_{ult}
Dimensionless load	V/As_u	H/As_u	M/ABs_u
Dimensionless ultimate load	V_{ult}/As_u	H_{ult}/As_u	M_{ult}/ABs_u
Normalised load	$v = V/V_{ult}$	$h = H/H_{ult}$	$m = M/M_{ult}$
Displacement	w	u	θ

horizontal capacity is independent of geometry with $H_{ult}/As_u = 1$. For all cases horizontal load governs failure for vertical loads less than approximately $0{\cdot}5V_{ult}$, and a pure sliding mechanism is observed in the region where $H = H_{ult}$. Fig. 4(b) shows the failure envelopes plotted in terms of normalised loads $v = V/V_{ult}$ and $h = H/H_{ult}$. The normalised envelopes fall in a very tight band, with the shape following the plane-strain plasticity solution proposed by Green (1954) (equation (4)). Expressed in terms of normalised loads v and h

$$v = 0{\cdot}5 + \frac{\cos^{-1} h + \sqrt{1 - h^2}}{2 + \pi} \tag{7}$$

where

$$h = 1 \quad \text{for} \quad v \leqslant 0{\cdot}5$$

The inclination factor given by equation (3) provides an algebraic fit to the VH envelope that can be expressed in terms of normalised loads to provide an alternative equation to the vh envelope

$$v = 0{\cdot}5 + 0{\cdot}5\sqrt{1 - h} \tag{8}$$

where

$$h = 1 \text{ for } v \leqslant 0{\cdot}5 \tag{8}$$

The VH failure envelope for a circular footing also follows the shape predicted by Green's solution (Gourvenec & Randolph, 2003). The apex points of the failure envelope for a circular footing are given by $V_{ult}/As_u = 6{\cdot}05$ (Cox *et al.*, 1961) and $H_{ult}/As_u = 1$. As such, under VH loading ($M = 0$) shape effects enhance the capacity of a footing with circular plan section more so than a square footing of equivalent area.

VM loading plane ($H = 0$)

Figure 5 shows failure envelopes under combined vertical and moment loading ($H = 0$) for footings unable to sustain tension, for aspect ratios $B/L = 0$, $0{\cdot}1$, $0{\cdot}2$, $0{\cdot}33$, $0{\cdot}5$, $0{\cdot}67$ and 1. The failure envelopes expand with increasing aspect ratio indicating increasing load capacity but, unlike in VH space, the envelopes in VM space expand along both load axes. Ultimate moment is mobilised in conjunction with a vertical load approximately half the uniaxial capacity, V_{ult}, at which point the swipe paths terminate (as shown in Fig. 5). Moment capacity diminishes with reducing vertical load, with no moment capacity available in the absence of vertical load. Constant-ratio displacement probe tests with high θ to low w indicated the failure envelope is symmetrical about $V = 0{\cdot}5V_{ult}$. The finite element swipe paths are compared with predictions from the effective width method and show reasonable agreement. A difference of $\sim$7% in ultimate moment is observed for plane-strain conditions, diminishing to 1% for a square footing.

Expressed in terms of normalised loads, Fig. 5(b) shows that the vm failure envelopes have a unique shape and are coincident with the effective width prediction. The shape of the normalised failure envelope can be described by a simple parabola

$$m = 4(v - v^2) \tag{9}$$

where $v = V/V_{ult}$ and $m = M/M_{ult}$.

Ultimate vertical load as a function of aspect ratio can be predicted from the quadratic expression given in equation (5). Ultimate moment capacity M_{ult} (from Fig. 5(a)) exhibits a linear relationship with aspect ratio that can be approximated by

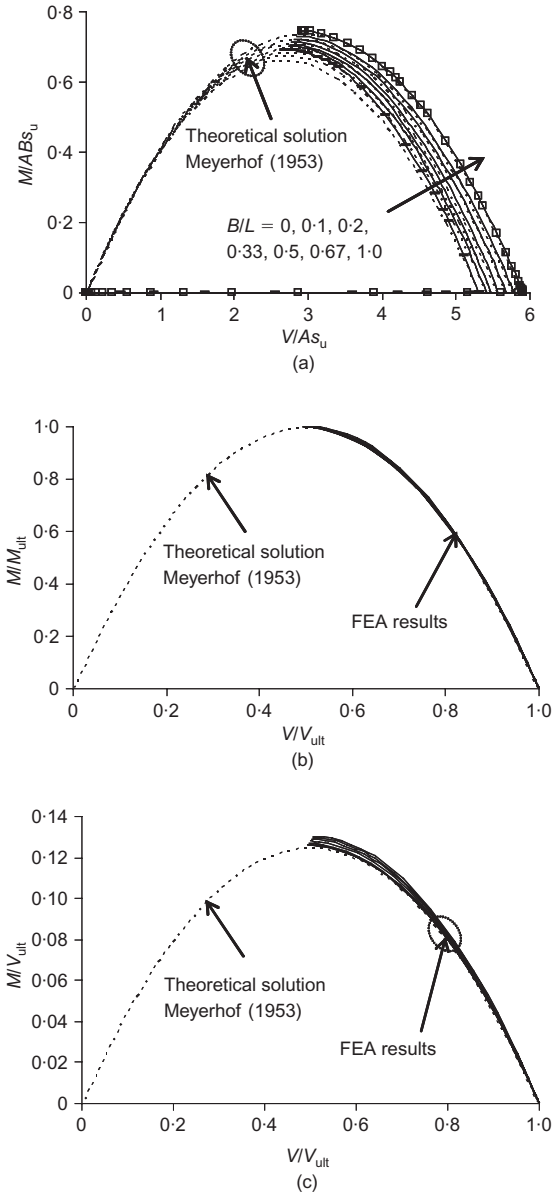

Fig. 5. Failure envelopes for VM loading ($H = 0$); zero-tension interface: (a) dimensionless load space; (b) normalised load space; (c) alternative normalised load space

$$\frac{M_{ult}}{ABs_u} = N_{cM} = M_{ult(B/L=0)} + 0{\cdot}05\frac{B}{L} \tag{10}$$

or expressed in terms of a moment shape factor

$$\frac{M_{ult}}{M_{ult(B/L=0)}} = s_{cM} = 1 + 0{\cdot}07\frac{B}{L} \tag{11}$$

$M_{ult(B/L=0)} = 0{\cdot}64$ predicted by the effective width method provides a safe estimate, as the method is essentially a lower-bound solution.

Alternatively the VM failure envelope can be represented with both vertical and moment loads normalised by V_{ult}, as shown in Fig. 5(c). The shape remains a simple parabola

$$m' = 0{\cdot}5(v - v^2) \tag{12}$$

where

$$m' = M/V_{ult}$$

In this case only equation (5) is required to scale the normalised envelope to failure loads $\{V/As_u,\ M/ABs_u\}$.

However, the size of the envelope decreases slightly with increasing aspect ratio, and the envelopes fall in a wider band than when normalised by their respective ultimate vertical and moment loads (as shown in Fig. 5(b)).

The *VM* failure envelope for a circular footing also follows the shape predicted by the effective width solution, provided an appropriate expression for effective area is used (Taiebat & Carter, 2003). In terms of absolute loads, the apex points of the failure envelope for a circular footing are given by $V_{ult}/As_u = 6{\cdot}05$ (Cox *et al.*, 1961) and $M_{ult}/As_u = 0{\cdot}57$ (Taiebat & Carter, 2003). The ultimate moment of a circular footing is less than in plane strain, so the *VM* failure envelope will cross over those shown in Fig. 5(a). Therefore, whether square or circular footing shape is optimum for *VM* loading ($H = 0$) depends on the dominant load component.

Figure 6 shows failure envelopes in vertical and moment load space ($H = 0$) for footings that can sustain unlimited tension, enabling the ultimate moment to be mobilised in conjunction with very low or zero vertical load. Represented in normalised load space (Fig. 6(b)) the failure envelopes do not fall on a unique curve (as when the interface is unable to sustain tension; see Fig. 5(b)); however, the shape can be described by the simple power law

$$v = (1 - m)^p \tag{13}$$

where

$$p = 0{\cdot}23 + 0{\cdot}1\frac{B}{L} - 0{\cdot}03\left(\frac{B}{L}\right)^2 \tag{14}$$

p ranges from 0·23 for plane strain to 0·3 for a square footing.

The ultimate moment capacity M_{ult} (from Fig. 6(a)) exhibits a linear relationship with aspect ratio that can be approximated by

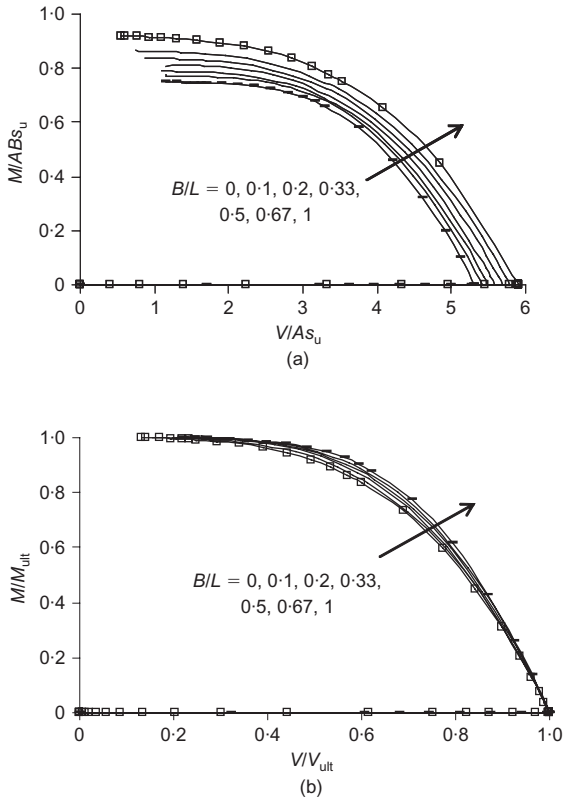

Fig. 6. Failure envelopes for *VM* loading ($H = 0$); unlimited tension interface: (a) dimensionless load space; (b) normalised load space

$$\frac{M_{ult}}{ABs_u} = N_{cM} = M_{ult(B/L=0)} + 0{\cdot}17\frac{B}{L} \tag{15}$$

or expressed in terms of a moment shape factor

$$\frac{M_{ult}}{M_{ult(B/L=0)}} = s_{cM} = 1 + 0{\cdot}22\frac{B}{L} \tag{16}$$

where $M_{ult(B/L=0)} = 0{\cdot}69$ from the plane-strain upper-bound solution for ultimate moment for a fully bonded footing (Murff & Hamilton, 1993, Randolph & Puzrin, 2003).

Upper-bound solutions are well established for moment capacity of strip and circular footings with unlimited tensile resistance, based on circular or spherical scoop mechanisms respectively (Murff & Hamilton, 1993; Randolph & Puzrin, 2003). Logic suggests that a cylindrical scoop will govern moment capacity of a rectangular footing, although spreading of the soil in the out-of-plane direction will prevent a prismatic mechanism developing. Fig. 7 shows the rotational failure mechanism ($H = 0$, $V = 0$) observed in the finite element analyses. In the plane of applied moment the mechanism observed through the mid-section and at the edge of the footing was independent of footing aspect ratio. Fig. 7(a) shows that the maximum depth of the scoop is $0{\cdot}288B$ beneath the footing/soil interface, giving a circular scoop with centre of rotation $0{\cdot}212B$ above the footing, which coincides with the optimal scoop mechanism for a plane-strain footing. Fig. 7(b) shows that the rotational failure under the edge of the footing (in the plane of applied moment) is no longer circular, and the depth of the scoop is reduced to $0{\cdot}235B$, approximately 20% less than at the mid-plane. The side view of the failure mechanism (Fig. 7(c)) shows that the scoop is generally prismatic, with the variation in depth of the rotational mechanism confined within $\sim 0{\cdot}2B$ of the edge of the footing, irrespective of the aspect ratio of the footing.

An upper-bound solution for rectangular footings based on a prismatic cylindrical slip plane with circular segments in the out-of-plane direction has been developed (Randolph, unpublished). A percentage of the work done on the out-of-plane sections can be defined to account for end effects. Fig. 8 compares the finite element predictions of ultimate moment capacity with upper-bound predictions with varying proportions of work done on the out-of-plane sections. A good fit is achieved between the finite element results and the upper bound by reducing the contribution of shearing on the out-of-plane sections to 40% of its full potential.

Equation (13) also represents the normalised shape of the *vm* failure envelope of a circular footing when $p = 0{\cdot}27$ (Gourvenec & Randolph, 2003a), which can be used in conjunction with the upper-bound solution $M_{ult(circle)} = 0{\cdot}67$ (Murff & Hamilton, 1993; Randolph & Puzrin, 2003).

VHM loading plane

Failure envelopes in planes of *HM* at $v = V/V_{ult} = 0{\cdot}25$, 0·5 and 0·75 for footings unable to sustain tension are shown in Fig. 9. The innermost envelope in Fig. 9(a) corresponds to plane-strain conditions ($B/L = 0$), the outermost envelope to a square footing ($B/L = 1$), and the intermediate envelope to a rectangular footing with $B/L = 2$. In normalised load space (Fig. 9(b)) the envelopes fall in a reasonably tight band and can be approximated as an ellipse symmetrical about $H = 0$.

The quasi-linear curves indicated by the dotted lines in Fig. 9(b) represent the failure envelopes predicted by equation (1). Conventional bearing capacity theory has been shown to provide a good representation of the failure envelopes in *vh* and *vm* load space (for footings unable to

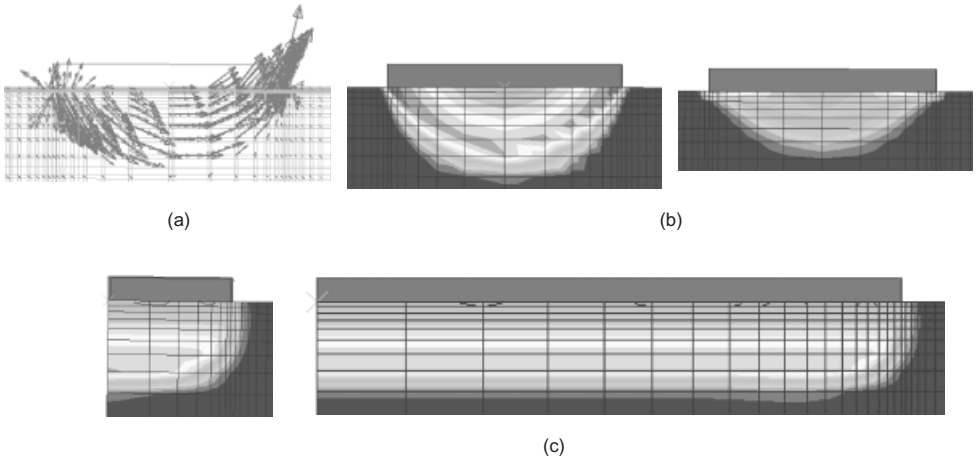

Fig. 7. Displacement vectors/contours at failure under pure moment for footings with unlimited tensile capacity: (a) at mid-section; (b) at edge; (c) longitudinal view, $L = B$ and $5B$

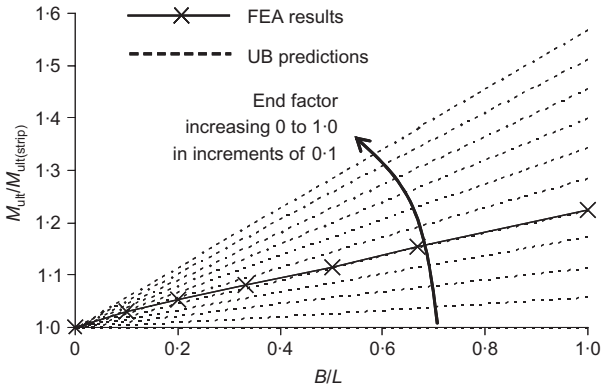

Fig. 8. Pure moment capacity for footings with unlimited tensile capacity

sustain tension), as shown in Figs 4(b) and 5(b). Fig. 9(b), however, indicates that coupling the separate solutions for load inclination and eccentricity leads to conservative predictions of ultimate limit states.

A new closed-form expression is proposed to define the normalised failure envelope explicitly as a function of v, m and h. Taking advantage of the elliptical nature of the failure envelopes in the HM plane, in terms of normalised loads the envelopes can be described by

$$\left(\frac{h}{h^*}\right)^2 + \left(\frac{m}{m^*}\right)^2 = 1 \tag{18a}$$

where h^* and m^* are functions of v and are derived from the shape of the failure envelopes in vh and vm space respectively (equations (8) and (9)).

Rearranging equation (8) as a function of h gives

$$h^* = \frac{0{\cdot}25 - (v - 0{\cdot}5)^2}{0{\cdot}25} \tag{18b}$$

and equation (9) directly gives

$$m^* = 4(v - v^2) \tag{18c}$$

Failure envelopes predicted by equation (18) are shown in Fig. 9(b) by the heavy broken lines. Equation (18) is presented graphically in vmh load space in Fig. 10, showing a scallop-shaped three-dimensional failure envelope.

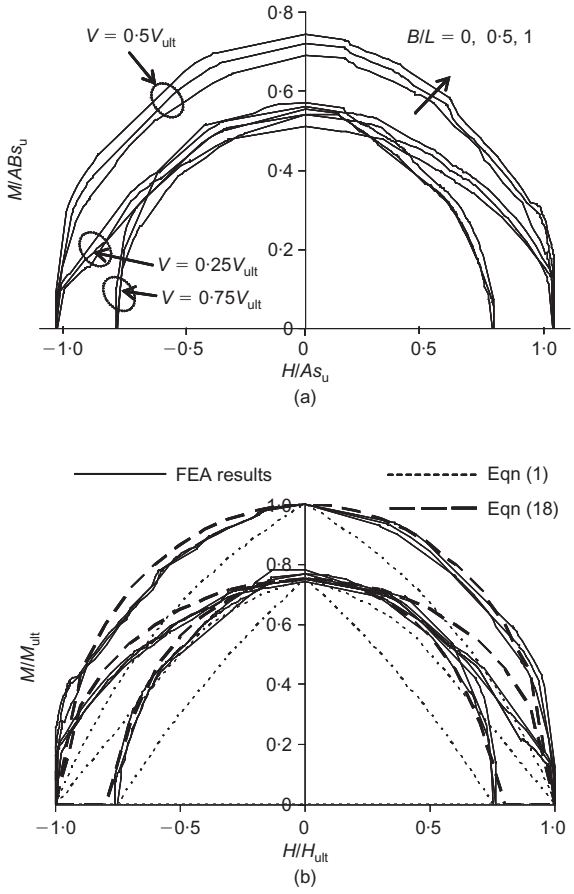

Fig. 9. Failure envelopes for VMH loading; zero-tension interface: (a) dimensionless load space; (b) normalised load space

It is interesting to note that the ultimate moment for a circular footing unable to sustain tension $M_{ult} = 0{\cdot}57/ABs_u$, mobilised at $V = 0{\cdot}5V_{ult}$, $H = 0$, is equivalent to the moment capacity for a square footing at the lower vertical load $V = 0{\cdot}25V_{ult}$ and $H = 0$ (Fig. 9(a)). As a result the failure envelope for a circular footing would lie well inside the failure envelope for either a rectangular or plane-strain footing, compensated for only by a minimal increase in vertical bearing capacity.

Figure 11 compares failure envelopes in planes of HM for footings permitted to mobilise unlimited tensile capacity for

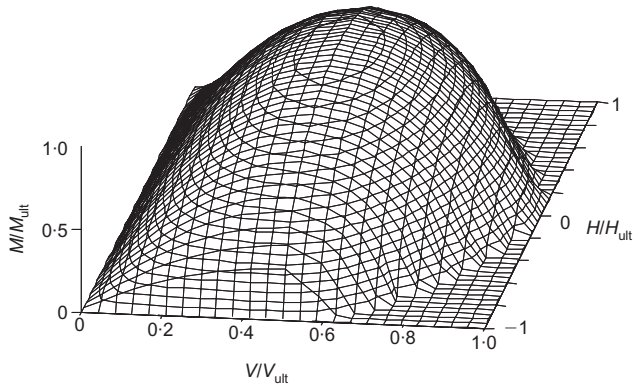

Fig. 10. 3D failure envelope for *VMH* loading; zero-tension interface

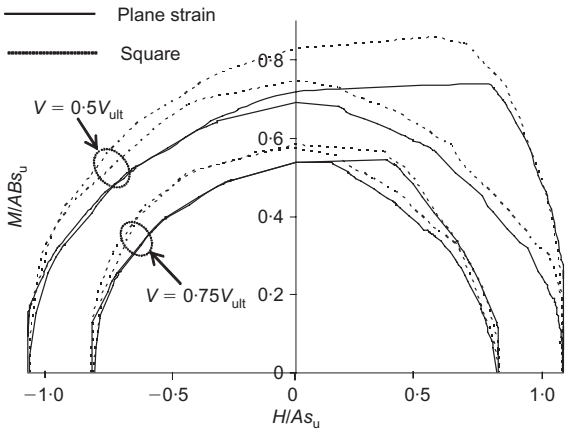

Fig. 12. Comparison of failure envelopes for *VMH* loading; zero-tension and unlimited tension interfaces

plane-strain and square geometry (i.e. $B/L = 0$ and 1). The failure envelope for a circular footing with unlimited tensile capacity from a previous study (Gourvenec, 2004) is also shown. Owing to the tensile resistance, moment capacity is available at zero vertical load (as observed in Fig. 6), and failure envelopes in planes of $v = 0$, 0·25, 0·5 and 0·75 are presented. Envelopes are asymmetric, with maximum moment mobilised in conjunction with horizontal load acting in the same direction (i.e. left to right with clockwise moment, or vice versa). The maximum moment of a square footing is mobilised under lower horizontal load than a circular footing or the plane-strain case. In all cases moment capacity diminishes rapidly following the peak. Fig. 11(b) shows that the shape of the failure envelope is a function of footing geometry and vertical load.

Taiebat & Carter (2000) propose a closed-form expression to describe the shape of the *vmh* failure envelope for a circular footing with an unlimited tension interface

$$v^2 + m(1 - \alpha hm)^2 + \left|h^3\right| = 1 \tag{19}$$

Envelopes predicted by equation (19) are shown in Fig. 11(b) by heavy broken lines.

Figure 12 compares failure envelopes in *HM* load space at constant vertical load $v = 0{\cdot}5$ and 0·75 for square and plane-strain footings with interfaces unable to sustain tension and with unlimited tensile capacity. Lower vertical load cases are not compared, as the moment capacities for the different interface conditions become increasingly incompatible. The additional potential capacity available if tensile resistance can be mobilised on the underside of the footing is most significant at lower vertical loads and when horizontal load and moment act in the same direction (i.e. left to right and clockwise, or vice versa). The envelopes for the two interface conditions are similar at higher vertical loads and when horizontal load and moment act in opposition (i.e. right to left and clockwise, or vice versa).

CONCLUSIONS

The aim of the work presented in this paper was to assess shape effects on the capacity of footings under general loading. Interface conditions either unable to sustain tension or able to mobilise unlimited tension have been considered.

Shape effects enhance the capacity of circular footings more so than footings of an equivalent area with a rectangular plan section when loading is predominantly vertical. When moment loads are significant, rectangular footing geometry becomes more efficient.

Vertical bearing capacity is related to the square of the footing aspect ratio (B/L), with a maximum increase of 15% available for a square footing ($B/L = 1$) relative to plane-strain conditions (equation (5)). In comparison, the bearing capacity factor for a circular footing is 18% greater than in plane strain. Moment capacity can be approximated as a linear function of footing aspect ratio, leading to a maximum

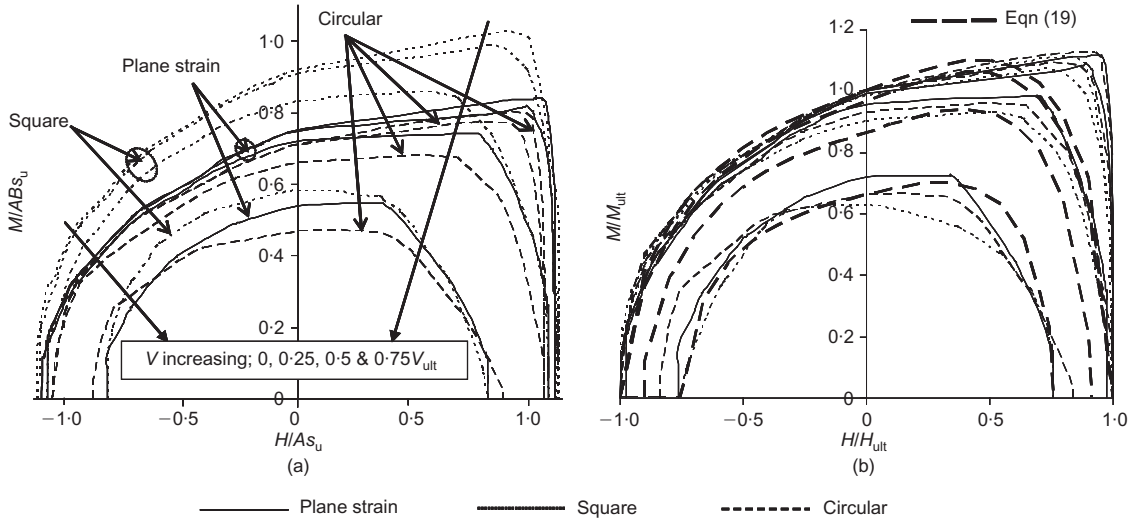

Fig. 11. Failure envelopes for *VMH* loading; unlimited tension interface: (a) dimensionless load space; (b) normalised load space

increase compared with plane-strain conditions of 7% and 22% for a square footing with zero-tensile capacity and unlimited tensile capacity respectively (equations (10) and (15)). In contrast, the moment capacity of a circular footing is 11% and 3% *less* than in plane strain for zero-tensile capacity and unlimited tensile capacity respectively. Horizontal capacity of a surface footing is independent of footing shape, being a function only of contact area and the undrained shear strength of the soil.

A unique shape is observed for failure envelopes for footings of varying aspect ratio under *VH* loading and *VM* loading for footings unable to sustain tension (Figs 4(b) and 5(b)). As a result, ultimate limit states for rectangular footings can be predicted from the theoretical plane-strain Green and Meyerhof solutions, or the algebraic expressions (equations (8) and (9)), scaled by appropriate uniaxial ultimate limit states. The failure envelope under *VM* loading of footings of varying aspect ratio with unlimited tensile capacity does not have a unique shape (Fig. 6(b)); the size of the normalised envelope decreases with increasing aspect ratio (i.e. as the footing gets shorter). As a result it would be unconservative to predict ultimate limit states for rectangular footings with tensile capacity by scaling the normalised envelope for plane-strain conditions. A simple power law is proposed to describe the shape of the normalised *vm* envelopes, with the exponent given as a quadratic function of footing aspect ratio (equations (13) and (14)).

Failure envelopes in planes of *HM* at constant *V* for footings unable to sustain tension are shown to be symmetrical ellipses (Fig. 9(a)), and their shape to be independent of footing aspect ratio (Fig. 9(b)). A closed-form expression is proposed to describe the shape of the normalised envelope in three-dimensional load space (equation (18)). The expression can be used in conjunction with equations (5) and (10) to predict ultimate limit states under any combination of *VMH* loading for a rectangular footing of any aspect ratio B/L. Predictions of ultimate limit states under general loading from conventional bearing capacity theory (equation (1)) are shown to be conservative (Fig. 9(b)).

The shape of the failure envelopes in *HM* space at constant *V* for footings with unlimited tensile capacity is not unique (Fig. 11(b)). The normalised envelopes for a square (or circular) footing fall within those for plane-strain conditions, indicating that it would be unconservative to predict ultimate limit states for a rectangular footing with tensile resistance by scaling a failure envelope derived for plane-strain conditions.

The capacity of a footing under load combinations involving horizontal load and moment acting in opposition (i.e. right to left to right and clockwise, or vice versa) is largely unaffected by the tensile capacity of the footing for vertical loads in excess of $0{\cdot}5V_{ult}$. For horizontal loads and moment acting in the same direction (i.e. left to right and clockwise, or vice versa) additional load capacity is available for footings able to mobilise tension (Fig. 12).

ACKNOWLEDGEMENTS

The work described here forms part of the activities of the Special Research Centre for Offshore Foundation Systems, established under the Australian Research Council's Research Centres Program. This support is gratefully acknowledged. The author would also like to thank Professor Mark Randolph for his advice on various aspects of the work presented in this paper.

NOTATION

A footing plan area
A' effective footing area ('effective area')
B footing breadth
B' effective footing breadth ('effective width')
H horizontal load
H_{ult} ultimate horizontal load
h normalised horizontal load (H/H_{ult})
i_c inclination factor
L footing length
M moment
M_{ult} ultimate moment
m normalised moment (M/M_{ult})
m' alternative normalised moment (M/V_{ult})
N_c bearing capacity factor
N_{cM} bearing capacity factor for moment
q_{ult} ultimate vertical bearing capacity
s_c shape factor
s_{cM} shape factor for moment capacity
s_u undrained shear strength
u horizontal displacement
V vertical load
V_{ult} ultimate vertical load
v normalised vertical load (V/V_{ult})
w vertical displacement
γ' effective unit weight

REFERENCES

Bransby, M. F. & Randolph, M. F. (1998). Combined loading of skirted foundations. *Géotechnique* **48**, No. 5, 637–655.

Butterfield, R. & Gottardi, G. (1994). A complete three-dimensional failure envelope for shallow footings on sand. *Géotechnique* **44**, No.1, 181–184.

Butterfield, R. & Ticof, J. (1979). Design parameters for granular soils (discussion contribution). *Proc. 7th Eur. Conf. Soil Mech. Found. Engng, Brighton* **4**, 259–261.

Butterfield, R., Houlsby, G. T. & Gottardi, G. (1997). Standardized sign conventions and notation for generally loaded foundations. *Géotechnique* **47**, No. 5, 1051–1054.

Cox, A. D, Eason, G. & Hopkins, H. G. (1961). Axially symmetric plastic deformation in soils. *Proc. R. Soc. London Ser. A* **254**, 1–45.

Gourvenec, S. (2004). Bearing capacity under combined loading: a study of the effect of shear strength heterogeneity. *Proc. 9th Australia New Zealand Conf. on Geomechanics, Auckland*, 527–533.

Gourvenec, S. & Randolph, M. F. (2003). Effect of strength nonhomogeneity on the shape and failure envelopes for combined loading of strip and circular foundations on clay. *Géotechnique* **53**, No. 6, 575–586.

Gourvenec, S., Randolph, M. F. & Kingsnorth, O. (2006). Undrained bearing capacity of square and rectangular footings. *Int. J. Geomech.* **6**, No. 3, 147–157.

Green, A. P. (1954). The plastic yielding of metal junctions due to combined shear and pressure. *J. Mech. Phys. Solids* **2**, No. 3, 197–211.

HKS (2002). *ABAQUS Users' Manual, Version 6·1*. Hibbit, Karlsson and Sorensen, Inc.

Levin, E. (1955). Indentation pressure of a smooth circular punch. *Q. Appl. Math.* **13**, No. 2, 133–137.

Martin, C. M. & Houlsby, G. T. (2001). Combined loading of spudcan foundations on clay: numerical modelling. *Géotechnique* **51**, No. 8, 687–699.

Meyerhof, G. G. (1953). The bearing capacity of foundations under eccentric and inclined loads. *Proc. 3rd Int. Conf. Soil Mech. Found. Engng, Zurich*, **1**, 440–445.

Michalowski, R. L. (2001). Upper bound load estimates on square and rectangular footings. *Géotechnique* **51**, No. 9, 787–798.

Murff, J. D. & Hamilton, J. M. (1993). P-ultimate for undrained analysis of laterally loaded piles. *J. Geotech. Engng Div. ASCE* **119**, No. 1, 91–107.

Nova, R. & Montrasio, L. (1991). Settlements of shallow foundations on sand. *Géotechnique* **41**, No. 2, 243–256.

Randolph, M. F. & Puzrin, A. M. (2003). Upper bound limit analysis of circular foundations on clay under general loading. *Géotechnique* **53**, No. 9, 785–796.

Roscoe, K. H. & Schofield, A. N. (1957). The stability of short pier foundations in sand: Discussion. *Br. Weld. J.*, January, 12–18.

Salgado, R., Lyamin, A. V., Sloan, S. W. & Yu, H. S. (2004) Two- and three-dimensional bearing capacity of foundations in clay. *Géotechnique* **54**, No. 5, 297–306.

Skempton, A. W. (1951). The bearing capacity of clays. *Proceedings of the Building and Research Congress*, London, Vol. 1, pp. 180–189.

Taiebat, H. A. & Carter, J. P. (2000). Numerical studies of the bearing capacity of shallow foundations on cohesive soil subjected to combined loading. *Géotechnique* **50**, No. 4, 409–418.

Taiebat, H. A. & Carter, J. P. (2002). A failure surface for the bearing capacity of circular footings on saturated clays. *Proc. 8th Int. Symp. Numerical Models in Geomechanics, NUMOG VIII, Rome*, 457–462.

Taiebat, H. A. & Carter, J. P. (2003). Contact between soil and circular foundations under eccentric loading. *Proc. 2nd MIT Conf. Computational Fluid and Solid Mechanics, Mass.*, 674–677.

Tan, F. S. (1990). *Centrifuge and theoretical modelling of conical footings on sand*. PhD thesis, Cambridge University, UK.

Terzaghi, K. (1943). *Theoretical soil mechanics*. New York: Wiley.

Ukritchon, B., Whittle, A. J. & Sloan, S. W. (1998). Undrained limit analysis for combined loading of strip footings on clay. *J. Geotech. Geoenviron. Engng ASCE* **124**, No. 3, 265–276.